Zhang, Z., Hu, B., Liu, F., Cheng, Y., Liu, X., Christensen, J. (2020). Pseudospin induced topological corner state at intersecting sonic lattices. *Physical Review B*, 101 (22), 220102(R), pp. 1-6.

DOI: https://doi.org/10.1103/PhysRevB.101.220102

Rapid Communications

Pseudospin induced topological corner state at intersecting sonic lattices

Zhiwang Zhang,[1] Bolun Hu,[1] Feng Liu,[2] Ying Cheng,[1,*] Xiaojun Liu,[1,†] and Johan Christensen[3,‡]

[1]*Department of Physics, MOE Key Laboratory of Modern Acoustics, Collaborative Innovation Center of Advanced Microstructures, Nanjing University, Nanjing 210093, China*

[2]*School of Physical Science and Technology, Ningbo University, Ningbo 315211, China*

[3]*Department of Physics, Universidad Carlos III de Madrid, ES-28916 Leganés, Madrid, Spain*

(Received 7 February 2020; revised manuscript received 18 May 2020; accepted 19 May 2020; published 2 June 2020)

Inspired by the discoveries of electronic topological phases and topological insulators, topologically protected boundary states in classical wave-based systems have attracted considerable interest in the last decade. Most recently, acoustic higher-order topological insulators and Kekulé-distorted sonic lattices have been proposed to support topological corner states and zero-dimensional bound states. Here, we demonstrate a domain wall induced topological corner state that is bound at the crossing point among finite acoustic graphenelike crystals. The approach is based on designing multipolar pseudospin resonances, which give rise to topologically trivial and nontrivial transitions across the domain walls that flank this unusual corner excitation toward the crossing point. By deliberately adding a substantial amount of defects into the cavities of the sonic lattice, we find that the pseudospin induced topological corner state remains entirely unaffected and pinned spectrally to the complete audible band gap. Our findings may thus have the potential to broaden the possibilities for sound confinement and focusing.

DOI: 10.1103/PhysRevB.101.220102

The discoveries of topological insulators [1,2] and topological semimetals [3] have sparked tremendous efforts during the last decade to conquer the analogous quantum effect in classical fields such as in optics [4–12], acoustics [13–27], and mechanics [28–36]. For example, acoustic one-dimensional (1D) boundary states in 2D systems, i.e., topological edge states, have been proposed in time-reversal symmetry broken structures to mimic the quantum Hall effect [13], pseudospins have been designed to emulate a quantum spin-Hall effect [16–19], and quantum valley-Hall phases have been engineered through the breaking of the mirror symmetry [20–22].

Moreover, analogous to the higher-order topological insulators [37–43] supporting the existence of lower-dimensional boundary states, acoustic second-order/third-order topological insulators sustaining 0D corner states in 2D/3D systems have been theoretically proposed and experimentally reported [44–50]. Besides these coveted corner states in higher-order topological insulators, bound states that confine energy tightly to topological defects have also been reported in the form of Majorana-like zero modes in Kekulé distorted lattices [51,52]. Most recently, independent reports demonstrated that domain wall induced topological corner modes can be obtained through combining pseudospin-orbit coupling and valley-projected physics [53,54]. In contrast to these two papers in photonics and mechanics, respectively, we predict for the first time the formation of domain wall induced topological corner states by intersecting topological insulators in acoustic systems through the sole deformation of the lattice without breaking the sublattice symmetry. The nonzero topological quadrupole guarantees the existence of the topological corner state in the bulk band gap. It is noted that the proposed platform is much easier to be fabricated compared with the previous proposals.

In this Rapid Communication, we design a quadripartite sonic crystal (QSC) hosting a 0D bound state at the crossing point of the orthogonal interfaces. We construct an acoustic graphenelike honeycomb lattice by connecting their "atoms," i.e., cavity resonators with each other through narrow coupling waveguides. Two spectrally distinct double Dirac cones (DCs) are formed in the acoustic band diagram whose frequencies are determined by the resonator structure constituting the sonic "metamolecule." Gapping and reclosing of the DCs can be straightforwardly obtained by varying the intra- and inter-metamolecular coupling strengths (t_{intra} and t_{inter}). We demonstrate that the topological phase is trivial when $t_{\mathrm{intra}} > t_{\mathrm{inter}}$ and nontrivial when $t_{\mathrm{intra}} < t_{\mathrm{inter}}$. On the basis of these constraints, we design a QSC containing two trivial and two nontrivial regions, forming a zigzag-type and a broken armchair-type interface along the y and x directions, respectively. Beyond the topological edge states that are induced by the pseudospin-orbit coupling, we predict highly defect-immune corner states at the center of the man-made QSC.

As shown in Fig. 1(a), we employ cylindrical cavity resonators of height $H = 41$ mm and radius $r = 20$ mm to construct the acoustic graphenelike honeycomb lattice. The metamolecule that contains six neighboring resonators is considered as the primitive cell with the lattice constant $a = 162$ mm as illustrated in Fig. 1(b). The intra- (t_{intra}) and inter- (t_{inter}) metamolecular coupling has been facilitated by

*chengying@nju.edu.cn
†liuxiaojun@nju.edu.cn
‡johan.christensen@uc3m.es

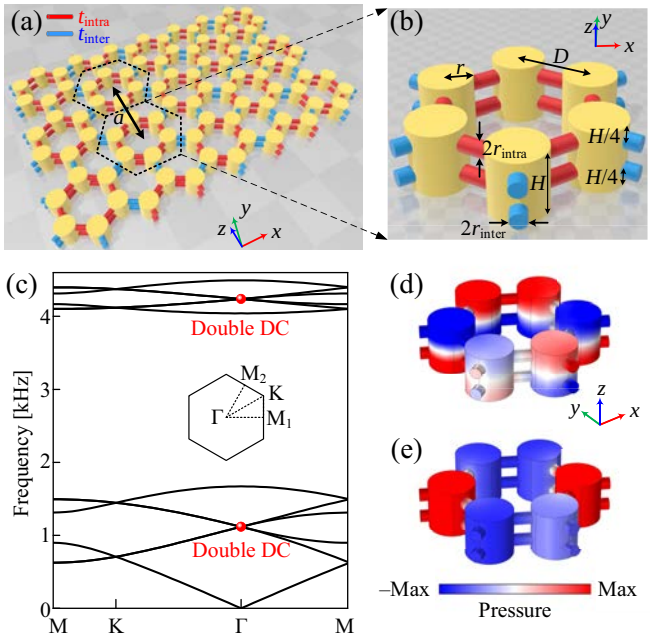

FIG. 1. (a) Schematic of the acoustic graphenelike honeycomb lattice, which is composed of identical cavity resonators (yellow) connected by variable coupling tubes (blue/red). (b) Enlarged view of the metamolecule. t_{intra} (t_{inter}) denote the intra- (inter-) metamolecular coupling strength that is controlled by the tube radius r_{intra} (r_{inter}). (c) Calculated band diagram of the lattice with $r_{intra} = r_{inter}$. Inset: First BZ. Pressure field of the acoustic modes corresponding to the (d) second and (e) first double Dirac cone. The color scale represents the total pressure field.

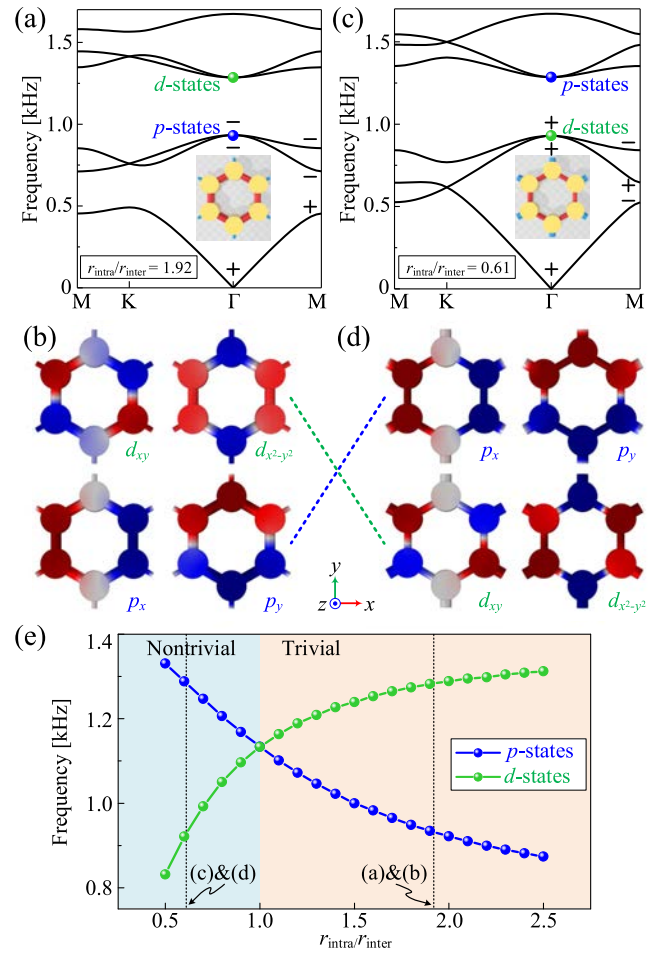

FIG. 2. (a) Band diagram of the honeycomb lattice where $r_{intra}/r_{inter} = 1.92$. Inset: Schematic of the trivial metamolecule. (b) Corresponding acoustic eigenmodes near the band gap at the Γ point. p_x and p_y display pseudospin dipole modes, while d_{xy} and $d_{x^2-y^2}$ mark pseudospin quadrupole modes, respectively. (c), (d) Same as (a) and (b), but for the nontrivial counterpart with $r_{intra}/r_{inter} = 0.61$. (e) Relationship between the eigenfrequencies of the double twofold degenerated states and the ratio r_{intra}/r_{inter}. The band inversion effect is clearly observed as indicated by different colors.

connecting parallel cylindrical waveguides (red and blue) at the positions $H/4$ and $3H/4$ of the resonators. By changing the radii of the waveguides one is able to alter their coupling strengths. For $r_{intra} = r_{inter} = r_0 = 5.2$ mm, which gives rise to uniform coupling $t_{intra} = t_{inter}$, we obtain two double DCs at the center of the first Brillouin zone (BZ), which are induced by the zone-folding mechanism of the honeycomb lattice [9,17]. The band diagram calculations have been obtained using the finite-element method, as shown in Fig. 1(c). In the simulations, hard boundary conditions are utilized when considering common acoustically rigid materials. We emphasize that there exist additional double DCs at even higher frequencies not shown here. Figure 1(d) illustrates the acoustic eigenmode of the second double DC. In each resonator, the acoustic pressure field vary sinusoidally along the z direction and behaves as an odd symmetric mode. On the contrary, the pressure field spreads homogeneously and symmetrically in the resonator at the first double DC [Fig. 1(e)]. In the ensuing analysis, we are going to design the acoustic QSC around the first double DC, whereas the discussion at higher frequencies is placed elsewhere [55].

Introducing disparity among intra- and inter-metamolecular coupling lifts the fourfold degeneracy of the double DC. For illustration, we design the acoustic honeycomb lattice with coupling strengths according to $r_{intra}/r_{inter} = 1.92$, which satisfies $2r_{intra}^2 + r_{inter}^2 = 3r_0^2$ to keep the entire volume of the structure unchanged, whose band diagram is shown in Fig. 2(a). We predict that these fourfold degenerated acoustic states of the topologically trivial lattice split into two twofold degenerated states and a complete bulk band gap is opened. The acoustic eigenmodes of these degenerated states at the Γ point are shown in Fig. 2(b). The pressure field inside the metamolecule exhibits a pair of pseudospin dipolar states below the band gap (bottom panels), which are even or odd symmetrical to the axes x/y similar to p_x/p_y-type orbitals. On the other hand, a pair of pseudospin quadrupolar states appear above the band gap (top panels), which are odd symmetrical to the axes x and y corresponding to a d_{xy}-type orbital, or even symmetrical to the axes x and y at the same time corresponding to $d_{x^2-y^2}$-type orbitals [17]. As shown in Fig. 2(c), the dispersion relation for the topologically nontrivial counterpart with coupling strengths $r_{intra}/r_{inter} = 0.61$ is computed. In this

scenario unlike the other, the corresponding eigenmodes shown in Fig. 2(d) display that the degenerated *p*-type states now appear above the *d*-type states, which means that a band inversion process has taken place in dependence of varying the intra- and inter-metamolecule coupling strengths [17,19]. This topological phase transition is best delineated by computing the bulk bands surrounding the topological gap as a function of the ratio of the involved waveguide radii $r_{\text{intra}}/r_{\text{inter}}$. Figure 2(e) illustrates this band inversion process between *p*-type and *d*-type states, which indicates the action at which the topological band gap is closed and reopened by changing the coupling strengths akin to the quantum spin-Hall effect. The dashed straight lines denote the geometrical coupling parameters that have been selected for the above trivial and nontrivial configurations, at which both acoustic graphenelike structures share the same bandwidth of the topological band gap.

The topological phase transition can be understood by the 2D Su-Schrieffer-Heeger (SSH) model and characterized by the dipole moment **P**. We demonstrate that the dipole moment can be determined by the eigenvalue of C_2 rotation at high-symmetric points according to [43]

$$P_i^n = \frac{1}{2}\left(q_i^n \text{ modulo } 2\right), \quad (-1)^{q_i^n} = \frac{\eta_n(M_i)}{\eta_n(\Gamma)}, \tag{1}$$

where $\eta^n(\mathbf{k})$ is the eigenvalue of C_2 rotation at the $\mathbf{k}$ point for the *n*th band, which is ± 1. Note that all of the eigenvalues at the high-symmetric points are labeled in Figs. 2(a) and 2(c). The corresponding acoustic eigenmodes below the band gap at the *M* point are illustrated in the Supplemental Material [55]. As a result, in the trivial case where $r_{\text{intra}}/r_{\text{inter}} = 1.92$, the dipole moments of all the three bands below the gap are 0. On the contrary, the dipole moments are $1/2$, 0, and $1/2$ for the first three bands, respectively, in the nontrivial case where $r_{\text{intra}}/r_{\text{inter}} = 0.61$. Due to the C_{6v} point group symmetry, the dipole moments satisfy $P_1^n = P_2^n$. The topological corner charge can be written by a quadrupole as [43]

$$Q_{ij}^c = \sum_1^n P_i^n P_j^n. \tag{2}$$

From Eqs. (1) and (2), the topological corner charges are $Q^c = 0$ in the trivial case and $Q^c = 1/2$ in the nontrivial case, respectively. The nonzero quadrupole guarantees the existence of the topological edge and corner states. We demonstrate that the procedure of achieving the topological corner state through tuning the inter-/intra-metamolecules coupling is universal for systems with such a topological phase transition, in spite of the different spectral locations related to the systems' specific structures and boundary conditions.

On the basis of the above knowledge, we construct a QSC that is made of four adjacent insulators capable to host domain wall induced topological edge states and corner mode confinements. As shown schematically in Fig. 3(a), the domain walls between trivial and nontrivial regions are orthogonal to each other, where the blue and magenta dashed lines denote the zigzag-type (interface I and interface III) and the broken armchair-type (interface II and interface IV) domain walls, respectively. The zigzag-type interface is parallel to the *y* axis and all the metamolecules remain intact. On the contrary,

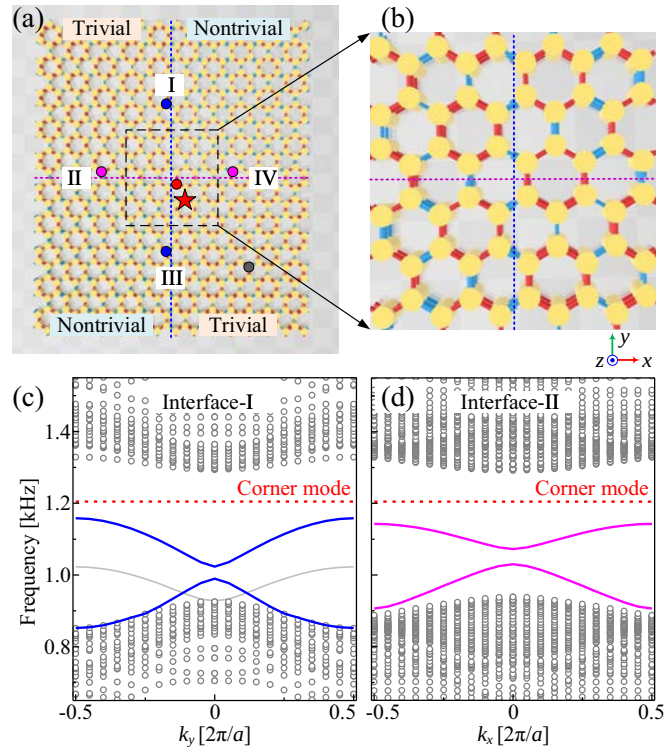

FIG. 3. (a) Schematic of the quadripartite sonic crystal comprising two different types of interfaces. The blue line denotes the zigzag-type interface while the magenta line corresponds to the broken armchair-type interface. (b) Enlarged view of the center region surrounding the dashed zone in (a). Projected band diagram simulations for ribbons having the interfaces of type (c) I and (d) II [see (a)]. The gray circles and lines represent the bulk and trivial edge states, respectively. The blue and magenta bands denote the topological edge states along their respective interfaces. The red dashed line marks the corresponding frequency of the corner mode.

the broken armchair-type interface is arranged along the *x* axis and the metamolecules near the interface are cut in half. The detailed difference between these two kinds of interfaces is discussed in the Supplemental Material [55]. In order to highlight the structure details, an enlarged view of the QSC center is depicted in Fig. 3(b). Projected dispersion relations along interface I and interface II are displayed in Figs. 3(c) and 3(d). Due to the time-reversal symmetry, the dispersion relations of interface III and interface IV, which are not shown here, are identical to those of interface I and interface II, respectively. Within the bulk band gap, pseudospin-dependent edge states have been highlighted by colored solid bands. These excitations are topologically protected as characterized by the spin-Chern number, corresponding to the acoustic analogous quantum spin-Hall effect [16,17]. The tiny gap between edge states is a consequence of the broken lattice symmetry at the interface [16,18]. Furthermore, it is worth mentioning the existence of a gap between the upper edge states and the bulk states.

We design the formation of domain wall induced topological corner states by introducing lattice deformations via the imbalance among the intra- and inter-metamolecular coupling strengths. The spectral location of these pseudospin induced

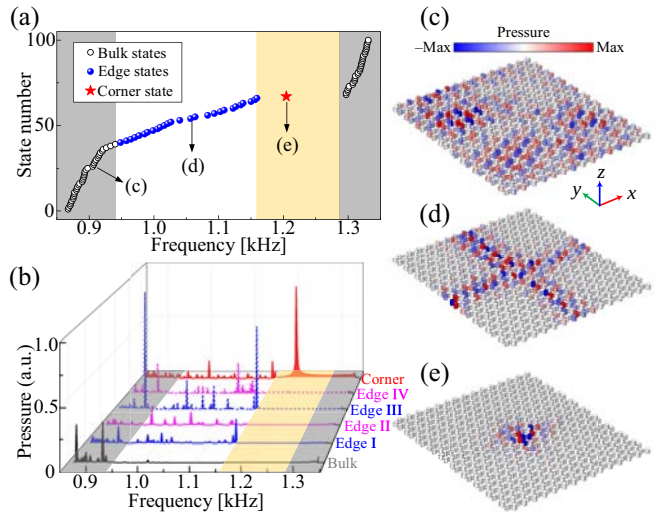

FIG. 4. (a) Calculated eigenfrequencies of the QSC. Black circles, blue dots, and red stars denote the bulk, edge, and corner states, respectively. (b) Detected pressure spectra for the bulk, edge, and corner states. Gray regions represent the bulk bands and the yellow one indicates the complete band gap. Corresponding eigenmodes of the (c) bulk, (d) edge, and (e) corner states as labeled in (a). Color represents the total pressure fields.

topological corner states is highlighted within the complete band gap as seen in Figs. 3(c) and 3(d). To verify the existence of the topological corner state, we calculate the eigenfrequencies of the QSC near the frequency of the first double DC. The QSC eigenfrequency spectrum in Fig. 4(a) unequivocally predicts the existence of bulk, edge, and corner state excitations. In order to unveil their spatial confinement rules, we conduct a transmission study of the modes by placing a monopolar point source at the center of the QSC as marked by the red star in Fig. 3(a). In the same sketch, additionally, we illustrate the sites of the state detection: The corner, edge, and bulk states are numerically measured at the red, blue/magenta, and gray dots, respectively. The transmission spectra are depicted in Fig. 4(b) whose respective peaks agree very well with the eigenvalue computations discussed in Fig. 4(a). The transmission peaks of the topological edge states can be clearly seen within the bulk band gap, but only the peak of the single corner state exists in the complete band gap. Specifically, all edge state excitations clearly reside within the bulk band gap. However, within the complete band gap from about 1.16 to 1.29 kHz (yellow region), a single corner state emerges. To shed more light on the spatial mode profile among the individual resonances, we compute their pressure distribution within the QSC. Undoubtedly, and as expected, the bulk waves distribute across the entire quadripartite sonic lattice as depicted in Fig. 4(c). However, according to the bulk-boundary correspondence, the topological protected edge states should appear within the bulk band gap and indeed sound waves confine along the orthogonal domain walls separating the trivial and nontrivial regions, which is confirmed in Fig. 4(d). The unique corner state that is indicated by the red star in the eigenvalue spectrum seen in Fig. 4(a) suggests to be spectrally situated right below the bulk bands and above the topological edge states as seen in the band diagrams of Figs. 3(c) and 3(d). Hence, beyond the bulk-boundary correspondence, we unravel another type of pseudospin induced corner state, whose pressure eigenfield, as depicted in Fig. 4(e), confines at the QSC center at which the domain walls cross. For comparison, eigenfrequency and eigenmode calculations for a QSC with two 120°-crossed zigzag-type interfaces are presented in the Supplemental Material [55], in which we conclude the absence of the topological corner mode.

The hallmark and defining feature of topological insulators is the resilience and robustness against disorder and defects in general. In order to corroborate the immunity to imperfections of the present QSC, we provide the smoking gun by a deliberate numerical defect analysis. We introduce "hard" perturbations to the QSC, by randomly inserting multiple acoustically rigid cylinders into the cavity resonators. The shaded green defect zone indicates the area in which we introduce these hard perturbations of the QSC [see Fig. 5(a)]. The analysis is conducted along two routes: First, we fix the geometry of such a single perturbation cylinder with a radius $r_p = 0.20r$ and height $H_p = H/5$, then we steadily increase the number of perturbation cylinders that are randomly located within the confines of the green zone. Figure 5(b) displays that the corner state at about 1.2 kHz hardly is affected by a growing number of defects. With up to 96 cylinders inserted, the spectral steadiness of the state underpins its topological robustness. The second analysis consists in keeping the aforementioned

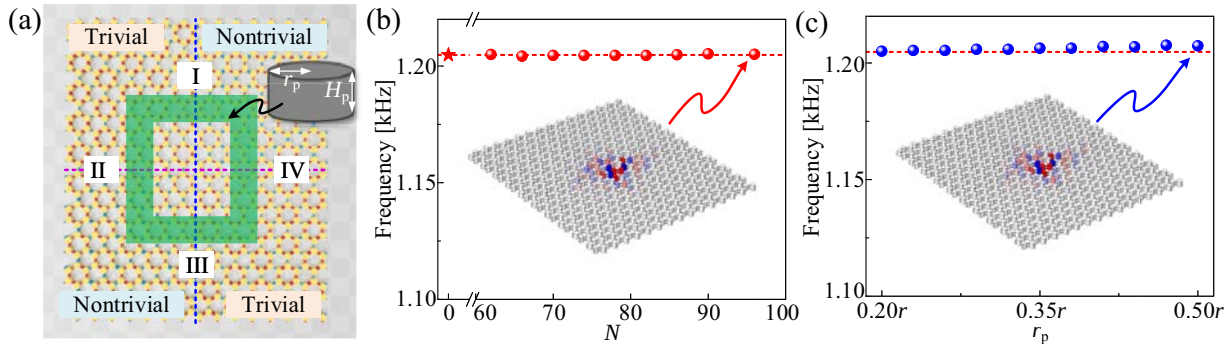

FIG. 5. (a) Within the shaded green (defect) zone, we introduce a number of rigid perturbation cylinders into the cavities where r_p and H_p are their radius and height. (b) Evolution of the corner states with the number of inserted cylinders N. (c) Same as (b), but here the radius of the perturbation cylinders r_p is increased. The red dashed line indicates the spectral location of the pristine corner state.

96 perturbation cylinders fixed at their sites, maintaining their heights, but now, as rendered in Fig. 5(c), we increase their radii r_p from $0.20r$ to $0.50r$. Again, the topological corner state remains unaffected by augmentation of the cylinder radii, however, for $r_p > 0.35r$, a slight frequency increase is predicted, which results from the resonance frequency shift of all defected cavities due to a decrease of the effective fluid volume therein. Despite this marginal drawback, pressure field simulations at extreme perturbation scenarios, i.e., $N = 96$ and $r_p = 0.5r$ as plotted in insets of Fig. 5(b) and Fig. 5(c), respectively, illustrate that sound remains highly concentrated at the QSC center of the crossing domain walls, which further reinforces the claim of excellent durability of the proposed corner mode excitation.

In summary, we presented an unparalleled corner state, whose origin cannot be explained via the common bulk-boundary correspondence. Instead, our approach rests on the design of man-made multipolar pseudospin modes in acoustic graphenelike honeycomb lattices, which give rise to a topological corner state at the intersecting domain walls separating the cavity-based sections of a finite quadripartite sonic crystal. To this end, we also demonstrate that the proposed corner state exhibits a convincing robustness against various introduced defects. Our results provide other ways to launch acoustic topological corner states that might lead to interesting sound concentration applications.

This work was supported by National Key R&D Program of China (Grant No. 2017YFA0303702), NSFC (Grants No. 11922407, No. 11834008, No. 11874215, and No. 11674172), Jiangsu Provincial NSF (BK20160018) and the Fundamental Research Funds for the Central Universities (Grant No. 020414380001). J.C. acknowledges the support from the European Research Council (ERC) through the Starting Grant No. 714577 PHONOMETA and from the MINECO through a Ramón y Cajal grant (Grant No. RYC-2015-17156).

[1] M. Z. Hasan and C. L. Kane, Rev. Mod. Phys. **82**, 3045 (2010).
[2] X.-L. Qi and S.-C. Zhang, Rev. Mod. Phys. **83**, 1057 (2011).
[3] X. Wan, A. M. Turner, A. Vishwanath, and S. Y. Savrasov, Phys. Rev. B **83**, 205101 (2011).
[4] F. D. M. Haldane and S. Raghu, Phys. Rev. Lett. **100**, 013904 (2008).
[5] Z. Wang, Y. D. Chong, J. D. Joannopoulos, and M. Soljačić, Phys. Rev. Lett. **100**, 013905 (2008).
[6] M. Hafezi, E. A. Demler, M. D. Lukin, and J. M. Taylor, Nat. Phys. **7**, 907 (2011).
[7] M. C. Rechtsman, J. M. Zeuner, Y. Plotnik, Y. Lumer, D. Podolsky, F. Dreisow, S. Nolte, M. Segev, and A. Szameit, Nature (London) **496**, 196 (2013).
[8] L. Lu, J. D. Joannopoulos, and M. Soljačić, Nat. Photonics **8**, 821 (2014).
[9] L.-H. Wu and X. Hu, Phys. Rev. Lett. **114**, 223901 (2015).
[10] J.-W. Dong, X.-D. Chen, H. Zhu, Y. Wang, and X. Zhang, Nat. Mater. **16**, 298 (2017).
[11] A. B. Khanikaev and G. Shvets, Nat. Photonics **11**, 763 (2017).
[12] T. Ozawa, H. M. Price, A. Amo, N. Goldman, M. Hafezi, L. Lu, M. C. Rechtsman, D. Schuster, J. Simon, O. Zilberberg *et al.*, Rev. Mod. Phys. **91**, 015006 (2019).
[13] Z. Yang, F. Gao, X. Shi, X. Lin, Z. Gao, Y. Chong, and B. Zhang, Phys. Rev. Lett. **114**, 114301 (2015).
[14] M. Xiao, G. Ma, Z. Yang, P. Sheng, Z. Zhang, and C. T. Chan, Nat. Phys. **11**, 240 (2015).
[15] Y.-G. Peng, C.-Z. Qin, D.-G. Zhao, Y.-X. Shen, X.-Y. Xu, M. Bao, H. Jia, and X.-F. Zhu, Nat. Commun. **7**, 13368 (2016).
[16] C. He, X. Ni, H. Ge, X.-C. Sun, Y.-B. Chen, M.-H. Lu, X.-P. Liu, and Y.-F. Chen, Nat. Phys. **12**, 1124 (2016).
[17] Z. Zhang, Q. Wei, Y. Cheng, T. Zhang, D. Wu, and X. Liu, Phys. Rev. Lett. **118**, 084303 (2017).
[18] Y. Deng, H. Ge, Y. Tian, M. Lu, and Y. Jing, Phys. Rev. B **96**, 184305 (2017).
[19] Z. Zhang, Y. Tian, Y. Cheng, X. Liu, and J. Christensen, Phys. Rev. B **96**, 241306(R) (2017).
[20] J. Lu, C. Qiu, L. Ye, X. Fan, M. Ke, F. Zhang, and Z. Liu, Nat. Phys. **13**, 369 (2017).
[21] Z. Zhang, Y. Tian, Y. Cheng, Q. Wei, X. Liu, and J. Christensen, Phys. Rev. Appl. **9**, 034032 (2018).
[22] Z. Zhang, Y. Tian, Y. Wang, S. Gao, Y. Cheng, X. Liu, and J. Christensen, Adv. Mater. **30**, 1803229 (2018).
[23] H. He, C. Qiu, L. Ye, X. Cai, X. Fan, M. Ke, F. Zhang, and Z. Liu, Nature (London) **560**, 61 (2018).
[24] X. Zhang, M. Xiao, Y. Cheng, M.-H. Lu, and J. Christensen, Commun. Phys. **1**, 97 (2018).
[25] F. Zangeneh-Nejad and R. Fleury, Phys. Rev. Lett. **122**, 014301 (2019).
[26] Z. Zhang, Y. Cheng, X. Liu, and J. Christensen, Phys. Rev. B **99**, 224104 (2019).
[27] P. Gao, Z. Zhang, and J. Christensen, Phys. Rev. B **101**, 020301(R) (2020).
[28] R. Süsstrunk and S. D. Huber, Science **349**, 47 (2015).
[29] S. H. Mousavi, A. B. Khanikaev, and Z. Wang, Nat. Commun. **6**, 8682 (2015).
[30] R. Chaunsali, E. Kim, A. Thakkar, P. G. Kevrekidis, and J. Yang, Phys. Rev. Lett. **119**, 024301 (2017).
[31] M. Miniaci, R. K. Pal, B. Morvan, and M. Ruzzene, Phys. Rev. X **8**, 031074 (2018).
[32] Y. Chen, X. Liu, and G. Hu, J Mech. Phys. Solids **122**, 54 (2019).
[33] J. Mei, J. Wang, X. Zhang, S. Yu, Z. Wang, and M.-H. Lu, Phys. Rev. Appl. **12**, 054041 (2019).
[34] G. Ma, M. Xiao, and C. Chan, Nat. Rev. Phys. **1**, 281 (2019).
[35] M. Miniaci, R. K. Pal, R. Manna, and M. Ruzzene, Phys. Rev. B **100**, 024304 (2019).
[36] Q. Zhang, Y. Chen, K. Zhang, and G. Hu, Phys. Rev. B **101**, 014101 (2020).
[37] W. A. Benalcazar, B. A. Bernevig, and T. L. Hughes, Science **357**, 61 (2017).
[38] W. A. Benalcazar, B. A. Bernevig, and T. L. Hughes, Phys. Rev. B **96**, 245115 (2017).
[39] J. Langbehn, Y. Peng, L. Trifunovic, F. von Oppen, and P. W. Brouwer, Phys. Rev. Lett. **119**, 246401 (2017).
[40] Z. Song, Z. Fang, and C. Fang, Phys. Rev. Lett. **119**, 246402 (2017).

[41] M. Ezawa, Phys. Rev. Lett. **120**, 026801 (2018).
[42] F. Schindler, A. M. Cook, M. G. Vergniory, Z. Wang, S. S. Parkin, B. A. Bernevig, and T. Neupert, Sci. Adv. **4**, eaat0346 (2018).
[43] F. Liu, H.-Y. Deng, and K. Wakabayashi, Phys. Rev. Lett. **122**, 086804 (2019).
[44] H. Xue, Y. Yang, F. Gao, Y. Chong, and B. Zhang, Nat. Mater. **18**, 108 (2019).
[45] X. Ni, M. Weiner, A. Alù, and A. B. Khanikaev, Nat. Mater. **18**, 113 (2019).
[46] Z. Zhang, M. Rosendo López, Y. Cheng, X. Liu, and J. Christensen, Phys. Rev. Lett. **122**, 195501 (2019).
[47] M. R. López, Z. Zhang, D. Torrent, and J. Christensen, Commun. Phys. **2**, 132 (2019).
[48] X. Zhang, H.-X. Wang, Z.-K. Lin, Y. Tian, B. Xie, M.-H. Lu, Y.-F. Chen, and J.-H. Jiang, Nat. Phys. **15**, 582 (2019).
[49] Z. Zhang, H. Long, C. Liu, C. Shao, Y. Cheng, X. Liu, and J. Christensen, Adv. Mater. **31**, 1904682 (2019).
[50] H. Xue, Y. Yang, G. Liu, F. Gao, Y. Chong, and B. Zhang, Phys. Rev. Lett. **122**, 244301 (2019).
[51] P. Gao, D. Torrent, F. Cervera, P. San-Jose, J. Sánchez-Dehesa, and J. Christensen, Phys. Rev. Lett. **123**, 196601 (2019).
[52] C.-W. Chen, N. Lera, R. Chaunsali, D. Torrent, J. V. Alvarez, J. Yang, P. San-Jose, and J. Christensen, Adv. Mater. **31**, 1904386 (2019).
[53] Y. Yang, Z. Jia, Y. Wu, R.-C. Xiao, Z.-H. Hang, H. Jiang, and X. Xie, Sci. Bull. **65**, 531 (2020).
[54] H. Fan, B. Xia, S. Zheng, and L. Tong, arXiv:1908.03476.
[55] See Supplemental Material at http://link.aps.org/supplemental/10.1103/PhysRevB.101.220102 for the discussions of the topological corner mode inspired by the higher-order resonance, acoustic eigenmodes at the *M* point, different types of interfaces, and QSC with two crossed zigzag-type interfaces.